Available online at www.sciencedirect.com
SCIENCE DIRECT®
Journal of Nuclear Materials 341 (2005) 103–114
journal of nuclear materials
www.elsevier.com/locate/jnucmat

Oxide dispersion-strengthened steels: A comparison of some commercial and experimental alloys

R.L. Klueh *, J.P. Shingledecker, R.W. Swindeman, D.T. Hoelzer

Metals and Ceramics Division, Oak Ridge National Laboratory, P.O. Box 2008, MS 6138, Oak Ridge, TN 37831, USA

Received 7 October 2004; accepted 6 January 2005

Abstract

Oxide dispersion-strengthened (ODS) steels are being developed and investigated for nuclear fission and nuclear fusion applications in Japan, Europe, and the United States. In addition, commercial ODS products are available and have been used in niche applications. Microstructural and mechanical properties studies have been conducted at Oak Ridge National Laboratory and elsewhere on various commercial and experimental ODS steels. Tensile and creep properties have been obtained and collected from literature and commercial sources. These data are compared to show the differences and similarities of different ODS steels, and observations are explained in terms of the microstructures of the steels.
Published by Elsevier B.V.

1. Introduction

If the conventional high-chromium ferritic/martensitic steels, such as modified 9Cr–1Mo and Sandvik HT9, or the reduced-activation steels, such as F82H, ORNL 9Cr-2WVTa, EUROFER, and JLF-1, were used for a fusion power plant first wall and blanket structure or for applications in Generation IV fission reactors, the upper operating temperature would be limited to 550–600 °C. Similar limitations are being realized in the use of ferritic/martensitic steels in fossil-fired plants. One way suggested to increase this limit to higher temperatures and maintain the advantages inherent in ferritic/martensitic steels (i.e. high thermal conductivity, low thermal expansion coefficient, and low void swelling during neutron irradiation relative to alternate elevated-temperature structural materials) is to use oxide dispersion-strengthened (ODS) steels. Elevated temperature strength in these steels is obtained through microstructures that contain a high density of small Y_2O_3 and/or TiO_2 particles dispersed in a ferrite matrix.

ODS steels are being developed and investigated for nuclear fission and fusion applications in Japan [1,2], Europe [3,4], and the United States [5,6]. Commercial ODS products are available and are being used in limited quantities; commercial alloys include MA956 and PM 2000 from Special Metals Corporation in the United States and Metallwerk Plansee GmbH in Germany, respectively. The MA957 discussed in this paper was developed by International Nickel Company (INCO), as was MA956. Although there is continued interest in MA957 for nuclear applications, there is presently no commercial source for the product.

* Corresponding author. Tel.: +1 865 5745111; fax: +1 865 241 3650.
E-mail address: kluehrl@ornl.gov (R.L. Klueh).

0022-3115/$ - see front matter Published by Elsevier B.V.
doi:10.1016/j.jnucmat.2005.01.017

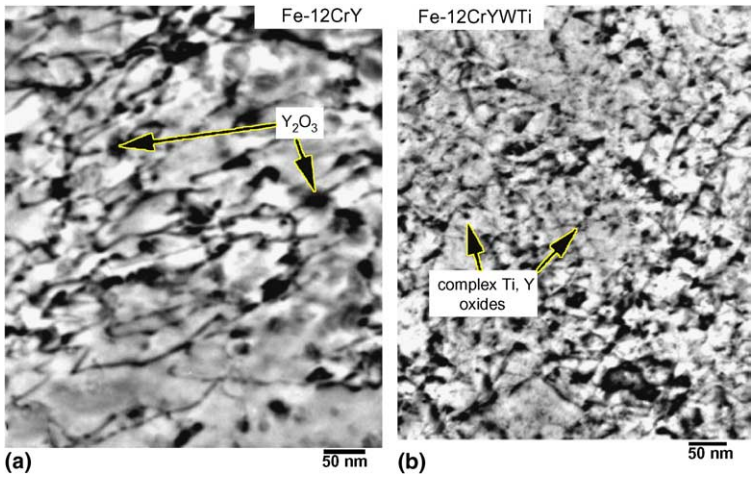

Fig. 1. Transmission electron micrographs of experimental ODS steels (a) 12Y1 (Fe–12Cr–0.25Y_2O_3) and (b) 12YWT (Fe–12Cr–2.5W–0.4Ti–0.25Y_2O_3).

In previous work at Oak Ridge National Laboratory (ORNL), the microstructures and tensile and creep properties of two experimental ODS steels with nominal compositions of Fe–12Cr–0.25Y_2O_3 (designated 12Y1) and Fe–12Cr–2.5W–0.4Ti–0.25Y_2O_3 (designated 12YWT) were investigated [7]. Optical microscopy, transmission electron microscopy (TEM) [8], and atom probe field ion microscopy [6,9] studies indicated that the 12Y1 microstructures were very different from those of 12YWT (Fig. 1). For 12Y1 (Fig. 1(a)), particles were estimated to be 10–40 nm in diameter at a number density of $10^{20} - 10^{21}$ m^{-3}; the dislocation density was estimated at $\approx 10^{15}$ m^{-2}. Diffraction studies indicated the particles were essentially pure, crystalline Y_2O_3. For 12YWT (Fig. 1(b)), dislocation density, particle size, and particle number density were estimated at 10^{15}–10^{16} m^{-2}, 3–5 nm diameter, and $1–2 \times 10^{23}$ m^{-3}, respectively. For this alloy, three-dimensional atom probe analysis revealed compositionally distinct nano-sized clusters enriched in Y, Ti, and O, slightly enriched in Cr, and slightly depleted in Fe and W.

These differences in microstructure were obviously the origin of the large differences in tensile and creep properties of the two steels [7]. Room-temperature yield stress of 12YWT was about 20% greater than 12Y1, but at 900 °C, the 12YWT was about 2.5 times as strong. This large difference at the highest temperatures translated into a much higher creep strength for the 12YWT [7].

In this paper, microstructural and mechanical properties studies at ORNL and elsewhere are presented, compared, and discussed to show the differences and similarities of different experimental (12Y1 and 12YWT) and commercial (MA956, MA957, and PM 2000) ODS steels. Implications of the mechanical property results from the commercial steels will be discussed in terms of microstructural observations.

2. Experimental procedure

Table 1 gives chemical compositions of the ODS steels to be discussed. Experimental alloys 12Y1 and 12YWT were produced in Japan by Kobe Special Tube Co. Ltd. PM 2000 is a commercial product of Metallwerk Plansee GMbH of Germany. The MA957 was

Table 1
Chemical compositions of ODS steels

Element*	12Y1	12YWT	MA956	MA957	PM 2000
C	0.045	0.050	0.03	0.030	0.01
Mn	0.04	0.60	0.06	0.09	0.11
P	<0.001	0.019	0.008	0.007	<0.002
S	0.002	0.005	0.005	0.006	0.0021
Si	0.03	0.18	0.05	0.04	0.04
Ni	0.24	0.27	0.11	0.13	0.01
Cr	12.85	12.58	21.7	13.7	18.92
Mo	0.03	0.02	<0.05	0.30	0.01
V	0.007	0.002			
Ti	0.003	0.35	0.33	0.98	0.45
Co	0.005	0.02	0.03		0.01
Cu	0.01	0.02			0.01
Al	0.007		5.77	0.03	5.10
B	0.004			0.0009	<0.0003
W	<0.01	2.44			0.04
Zr	0.003				<0.01
N	0.017	0.014	0.029	0.044	0.0028
O	0.15	0.16	0.21	0.21	0.25
Y	0.20	0.16	0.38	0.28	0.37

* Balance iron.

manufactured by INCO Metals, and MA956 is a product of Special Metals Corporation.

General processing of all the ODS alloys involved mechanical alloying, compaction, and extrusion, after which they were processed into the final geometry and given a final recrystallization heat treatment. For the commercial alloys, detailed processing procedures were not available. The processing procedures involved in producing ODS steels can be illustrated by describing the processing used for the experimental 12Y1 and 12YWT alloys produced by Kobe Steel. These alloy compositions were prepared by mechanical alloying of argon-gas-atomized 70-μm diameter pre-alloyed metal powder with 20-nm Y_2O_3 powder in a high-energy attritor in an argon atmosphere for 48 h. Mechanically alloyed flakes were then degassed 2 h at 400 °C in vacuum, after which they were canned in mild steel and hot extruded at 1150 °C into bar. The 12Y1 and 12YWT bars were hot rolled at 1150 °C to 7-mm plate. The 12Y1 plate was cold rolled to 2 mm, and the 12YWT was warm rolled at 600 °C to this thickness. Warm rolling was used for the 12YWT because of its higher strength. Both alloys were given a final anneal of 1 h at 1050 °C in vacuum.

Results from tensile and creep tests conducted at ORNL on the experimental alloys 12Y1 and 12YWT were previously reported [7]. Creep tests were conducted at ORNL on the commercial steels MA957 [10] and PM 2000 [11]. For comparison, data were also taken from literature or vendor data sheets for creep and tensile behavior of MA956 [5,12], MA957 [13,14] and PM 2000 [15]. Creep tests at ORNL on 12Y1 and 12YWT were conducted at 600–900 °C, those on MA957 were at 800–925 °C, those on MA957 were at 800–925 °C, and those on PM 2000 at 850–1000 °C. Vendor data were at 800–1150 °C for MA956 [12], at 650 °C for MA957 [13], and 900–1200 °C for PM 2000 [15]. All mechanical-property data are for specimens taken in the worked direction–the high-strength direction. Tests were conducted in air.

Different product forms for the different alloys were used in the creep and tensile tests at ORNL. The 12Y1 and 12YWT specimens were from 2-mm sheet, MA957 specimens were from a tube 65-mm OD with a 25-mm wall thickness, and the PM 2000 specimens were from 0.08- and 0.13-mm sheet.

3. Results

3.1. Tensile behavior

Yield stress and ultimate tensile strength data for the experimental 12Y1 and 12YWT steels over the range room temperature to 900 °C are shown in Fig. 2, along with data for a non-ODS reduced-activation steel, ORNL 9Cr-2WVTa [16]. The obvious strength advantage of 12YWT is evident.

Of the commercial ODS steels, the MA957 had the highest yield stress and ultimate tensile strength, and the MA956 had the lowest values (Fig. 3). In fact, up to 700 °C, the yield stress of the MA956 was less than that of 9Cr-2WVTa – a non-ODS martensitic steel. The strength of PM 2000 fell between the values for the MA956 and MA957.

When the commercial steels are compared with the experimental steels (Fig. 4), the MA957 and 12YWT, the strongest of the commercial and experimental steels, respectively, have similar strengths. The 12Y1 is similar to PM 2000 at low temperatures, but it then approaches the values for MA956 at the higher temperatures. All steels appear to approach a common low-strength value as the temperature is increased to 900 °C.

Minor differences were observed in the total elongations of the experimental and commercial steels (Fig. 5). The 12Y1 and 12YWT had the lowest values at room temperature, and the 12Y1 had the highest values between 600 and 800 °C. Otherwise, the elongations of the commercial steels and the 12YWT were comparable.

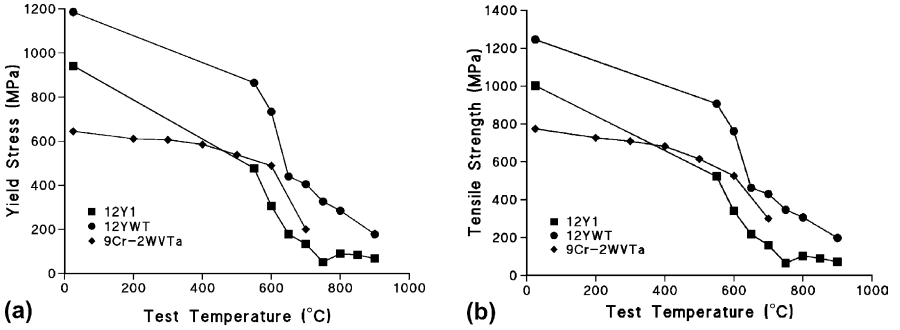

Fig. 2. (a) Yield stress and (b) ultimate tensile strength as a function of test temperature for the experimental ODS steels 12Y1 and 12YWT compared to the non-ODS reduced-activation steel ORNL 9Cr-2WVTa.

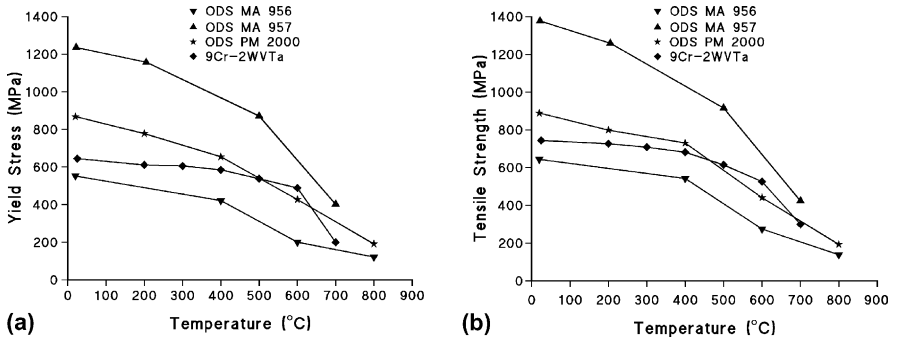

Fig. 3. A comparison of the (a) yield stress and (b) ultimate tensile strength as a function of test temperature for the three commercial ODS steels and the non-ODS reduced-activation steel ORNL 9Cr-2WVTa.

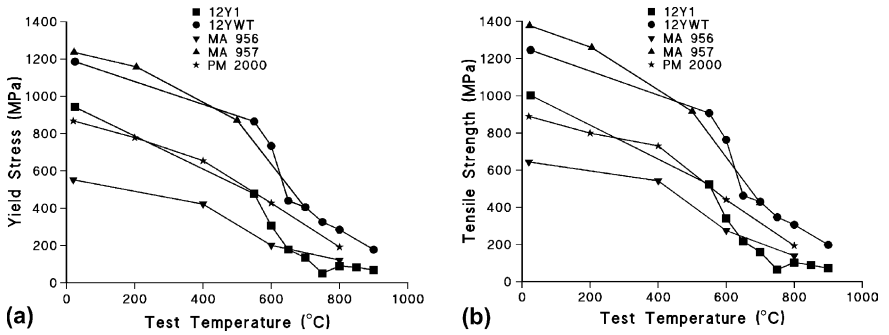

Fig. 4. A comparison of (a) yield stress and (b) ultimate tensile strength as a function of test temperature of the experimental and commercial ODS steels.

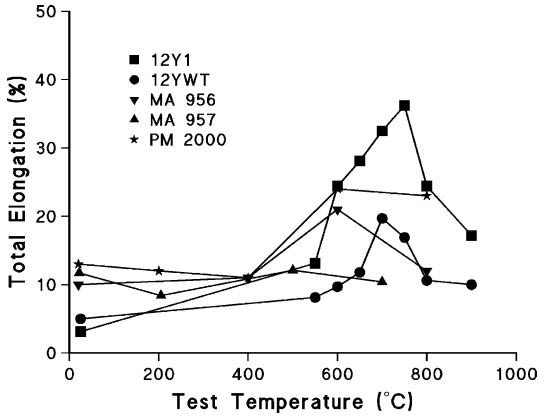

Fig. 5. A comparison of the total elongation as a function of test temperature of the experimental and commercial ODS steels.

3.2. Creep-rupture behavior

Creep-rupture behavior of the different steels was compared using a Larson–Miller Parameter (LMP) with a constant of 25, which was used for MA956 and MA957 previously [5]. A comparison of the experimental steels (Fig. 6) showed the superiority of the 12YWT to the 12Y1, in agreement with the yield stress behavior. Also shown in Fig. 6 are data for a conventional 9Cr-WMoVNb steel (a commercial steel designated NF616 or Grade 92). The creep behavior of the 12Y1 was similar to that of the conventional steel.

Comparison of the creep-rupture properties of the experimental ODS steels with the strongest (highest yield stress) commercial ODS steel MA957 and the weakest commercial ODS steel MA956 indicates that MA956 and 12YWT have similar properties at high LMP. At low LMP, MA956 and MA957 are weaker than 12YWT (Fig. 7). Over the range where the LMP data for MA957 and MA956 overlap, they appear to approach similar values, indicating an eventual convergence of the data for MA957 and 12YWT, although that still needs to be demonstrated.

A comparison of the LMP values for creep tests at ORNL on the PM 2000 sheet with the experimental steels (Fig. 8) indicates that the creep-rupture strength of PM 2000 is as good as that of 12YWT for the conditions tested. For the different sheet thicknesses, the thinner 0.08-mm sheet had better properties than the

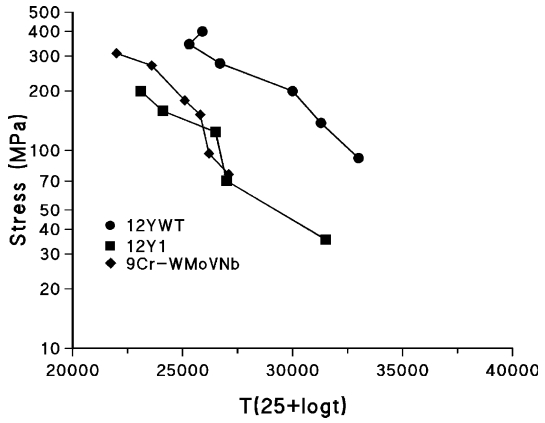

Fig. 6. Rupture stress vs. Larson–Miller parameter for the experimental ODS steels 12Y1 and 12YWT and a conventional non-ODS steel NF616 (9Cr-WMoVNb).

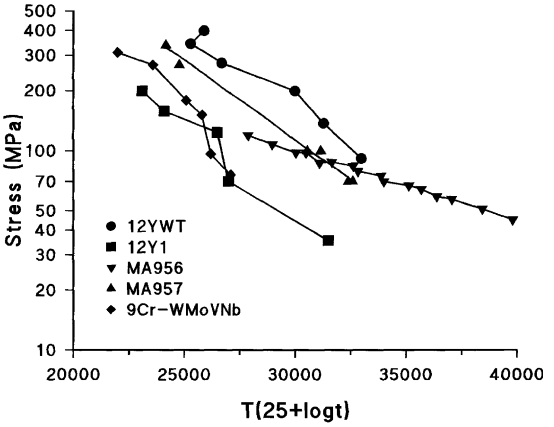

Fig. 7. Rupture stress vs. Larson–Miller parameter for the commercial steels MA956 and MA957 compared to the experimental ODS steels and a non-ODS steel.

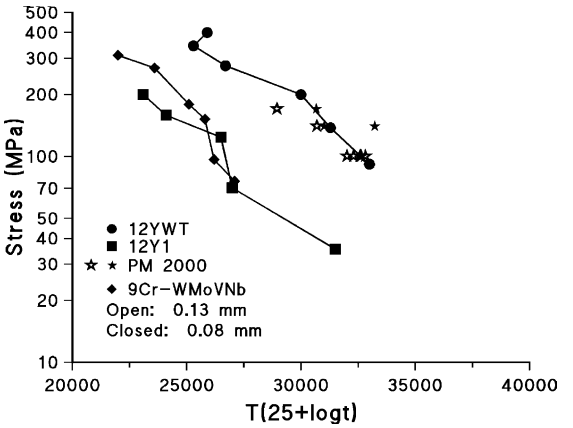

Fig. 8. Rupture stress vs. Larson–Miller parameter for the commercial PM 2000 0.08- and 0.13-mm sheet tested at ORNL compared to the experimental ODS steels and the non-ODS steel.

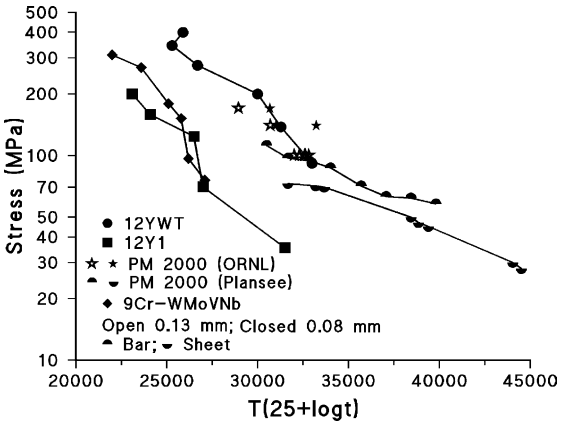

Fig. 9. Rupture stress vs. Larson–Miller parameter for the commercial PM 2000 data 0.08- and 0.13-mm sheet tested at ORNL and data taken from the vendor (Plansee) on bar and sheet compared to the experimental ODS steels and the non-ODS steel.

0.13-mm sheet. This evaluation is further strengthened when the ORNL data are compared with those from the vendor (Plansee) data sheet for bar and sheet (Fig. 9) [15]. In this case, the bar was the strongest, but both products for the high-temperature tests conducted indicated a tendency similar to the MA956 for high LMPs. When all the ODS steel data are compared (Fig. 10), all but the 12Y1 appear to approach similar values for high LMP (low-stress and/or high temperature tests). This occurs despite the quite different yield stress values for the different steels.

3.3. Microstructures

Optical microscopy of the three commercial (Fig. 11) and two experimental (Fig. 12) ODS steels were examined. The anisotropy present in each of the steels is obvious from these photomicrographs, as is the variation of grain size. The MA956 had a relatively large grain size, while the PM 2000 had a relatively small grain size. The 12YWT was not completely recrystallized [dark regions in Fig. 12(b) are unrecrystallized]. The MA957 and PM 2000 contained unrecrystallized regions, but it was difficult to determine how much. It appeared that MA956 was completely recrystallized. Microstructures of all the steels showed indications of large second-phase particles, usually aligned in the rolling direction, that were not related to the fine oxide particles that give ODS steels their strength. The particles probably limit the strength of the steels, and in this study, these features in MA957 were examined and are discussed in the following.

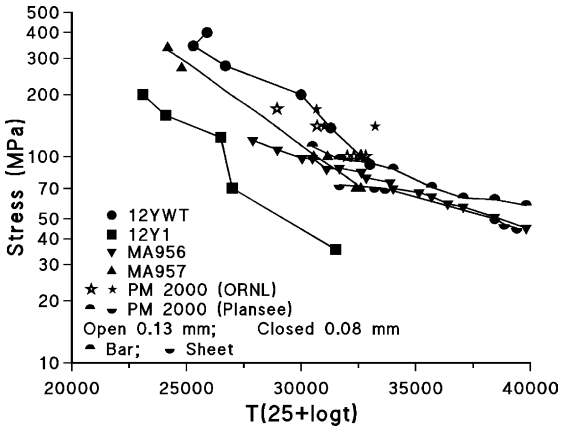

Fig. 10. Rupture stress vs. Larson–Miller parameter for all the commercial and experimental ODS steels.

Detailed optical microscopy of the MA957 revealed large second-phase particles that often appeared as relatively large 'stringers' (Fig. 13) aligned along the rolling direction. A failed creep-rupture specimen was examined, and the failure appeared to be associated with the stringer material (Fig. 14). That is, it appeared that cavities formed in conjunction with the particles of stringer material and other extraneous particles not in the stringers, and these cavities linked up perpendicular to the worked direction (parallel to the eventual fracture surface).

To determine the nature of the particles in the stringers and other extraneous particles (not the fine distribution of oxide particles that strengthen ODS steels), the gage section of the creep-rupture specimen shown in Fig. 14 was examined by scanning electron microscopy (SEM) with a field emission gun (FEG) using backscattered and secondary electrons (Fig. 15). Such large particles are expected to be deleterious to the mechanical properties.

As expected, the primary elements identified in the matrix of the MA957 were Fe, Cr, and Ti. The extraneous particles in and out of the stringers were rich in sev-

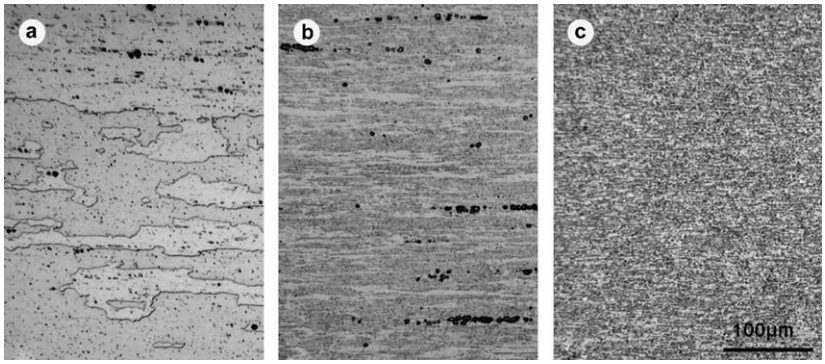

Fig. 11. Photomicrographs of commercial ODS steels: (a) MA956 plate, (b) MA957 tube, and (c) PM 2000 rod.

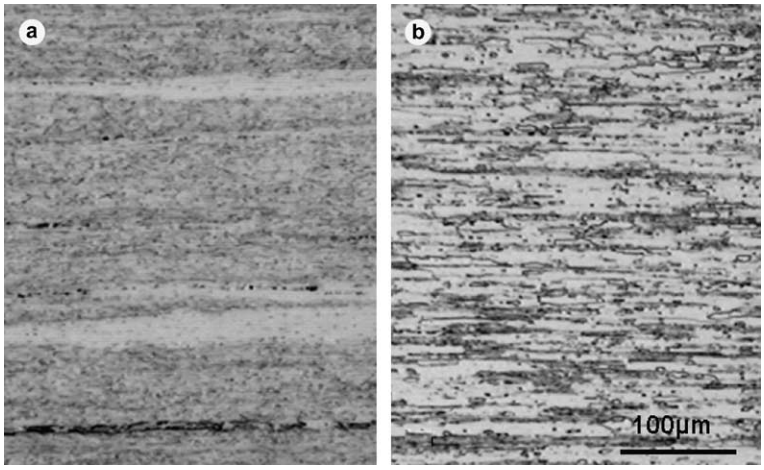

Fig. 12. Photomicrographs of experimental ODS steels: (a) 12Y1 and (b) 12YWT.

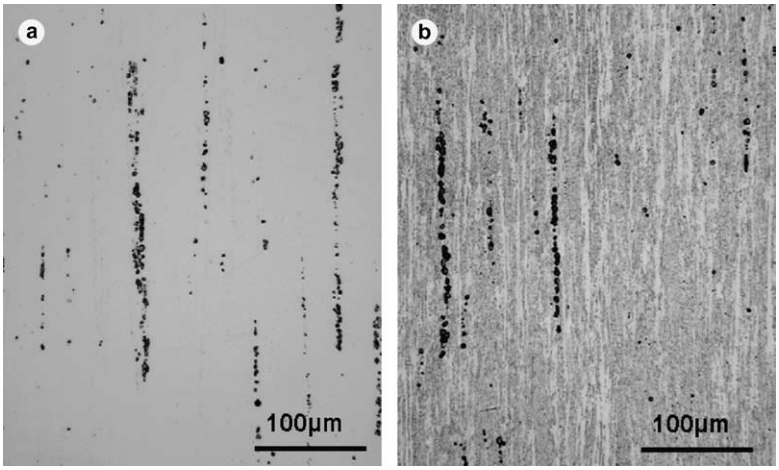

Fig. 13. Optical microstructure of MA957 ODS steel (a) as polished and (b) etched.

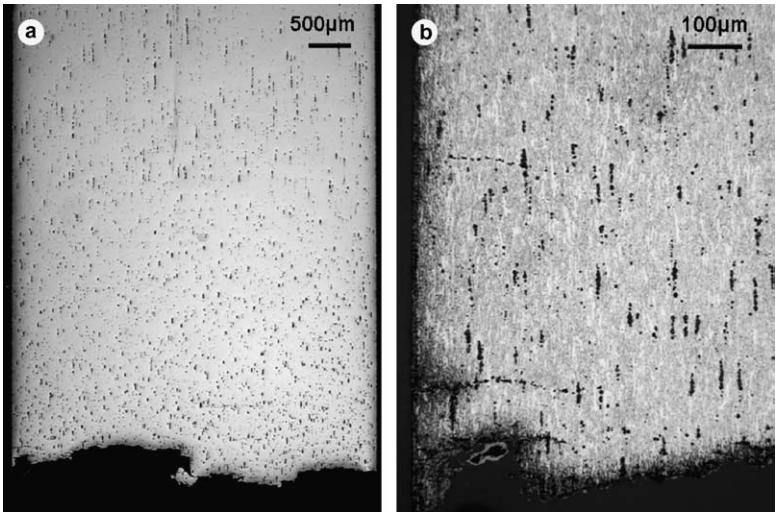

Fig. 14. Optical micrographs at two different magnifications of creep-rupture specimen of MA957 tested at 100 MPa at 900 °C that ruptured in 36.7 h: (a) unetched and (b) etched.

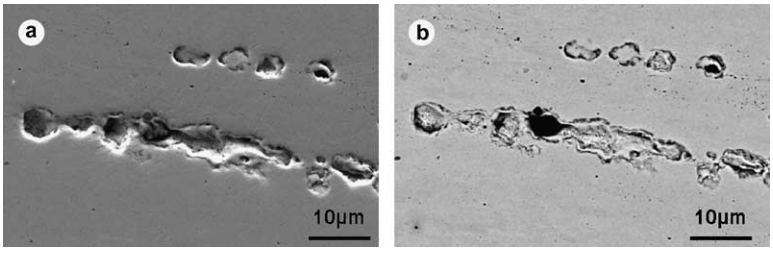

Fig. 15. Scanning electron microscopy (a) secondary electron image and (b) backstattered electron image (compositional contrast) of 'stringers' in gage length of MA957 creep specimen.

eral different elements. Many particles in the stringers were carbon rich (Fig. 16); the presence of carbon is probably the result of mill contamination during the mechanical alloying process. Small precipitates

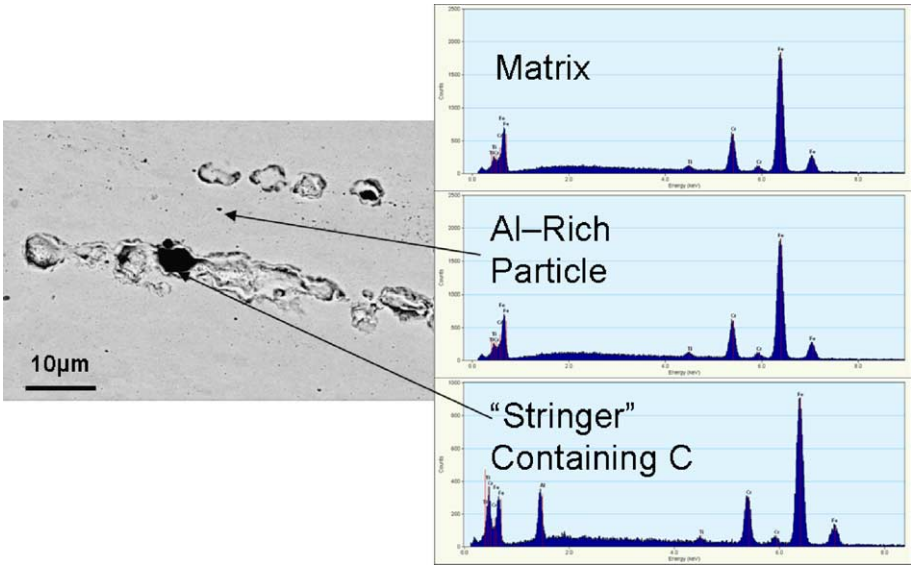

Fig. 16. Results of scanning electron microscopy backscattered image analyses that show the presence of high carbon and aluminum enrichment in the large particles present in the ODS steel MA957.

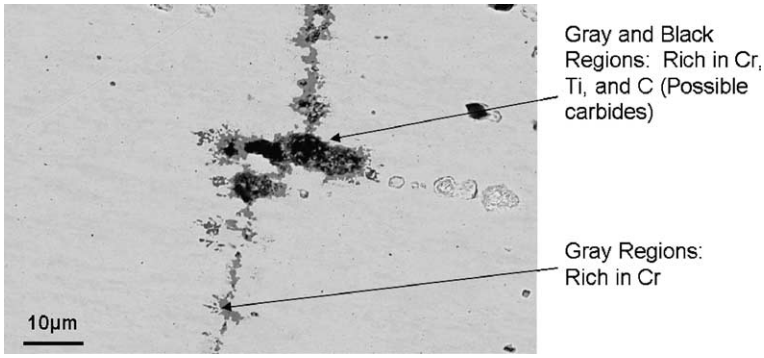

Fig. 17. Scanning electron microscopy backscattered image showing that segregation occurs perpendicular to the worked direction in the region of the creep fracture.

throughout the microstructure were found to be aluminum rich (Fig. 16). Aluminum is probably also from mill contamination, since the specification for MA957 does not contain aluminum.

Examination of a region near the creep failure indicated the presence of segregation that links up regions between stringers (Fig. 17) and probably leads to the relatively brittle creep failure shown in Fig. 14. The segregation, especially in the stringers, is rich in chromium, titanium, and carbon, which probably indicates the presence of carbide particles. These particles in the stringers were joined by 'trails' of segregation that were found to be chromium rich. There were also indications of cavitation associated with areas of the segregation, indicating that it could be the joining of such cavitation that leads to the creep failure.

4. Discussion

Development of ODS steels for fast reactor cladding began in Belgium in the late 1960s [18], and work for that application has continued over the years [1,2,19–21]. The main problem keeping the steels from being used for that application is anisotropy in properties resulting from the fabrication process. Fabrication involves mechanical alloying of metal alloy powders with oxide (Y_2O_3) powders, followed by compaction, and then extrusion at an elevated temperature. The steels have superior creep strength in the longitudinal (extrusion) direction (properties most often studied), but, in the case of tubes, not in the biaxial direction. The problem with anisotropy still exists in the recent steels being developed [19–22], although there have been advances in

reducing it [23]. Anisotropy is present in the microstructures of the steels discussed in this paper (Figs. 11 and 12), although that subject will not be discussed further. The objective of these studies was to compare strength properties in the strong (longitudinal) direction to determine similarities and differences among the different commercial and experimental steels that have been studied recently.

The TEM examination at ORNL of the experimental Fe–12.3Cr–3W–0.39Ti–0.25Y_2O_3 (12YWT) and an Fe–12.4Cr–0.25Y_2O_3 (12Y1) ODS steels indicated that the 12YWT contained 3–5-nm diameter particles at a number density of $1–2 \times 10^{23}$ m^{-3}, whereas the 12Y1 contained 10–40 nm particles at a number density of 10^{20}–10^{21} m^{-3} (Fig. 1) [8]. There was also a lower dislocation density in the 12Y1, and it was more fully recrystallized than 12YWT. Electron diffraction indicated that particles in the 12Y1 were essentially pure Y_2O_3. Because of the small size of the particles in 12CrYWT, the three-dimensional atom probe (3-DAP) was required to determine that the small particles were primarily atom clusters enriched in Y, Ti, and O [6,9]. From this [6,9] and previous work [24], it was concluded that the original Y_2O_3 particles dissolved during mechanical alloying, and atom clusters as small as 2-nm in diameter formed during subsequent processing (extrusion, etc.). Particle dissolution and subsequent reformation was obvious, since the atom probe indicated that the concentration of titanium in the high-oxygen clusters was higher than the concentration of yttrium, which was introduced by the addition of Y_2O_3 [6,9]. The presence of the high titanium concentration in the atom clusters indicated that it played a role in the dissolution of the Y_2O_3, and this is the reason that the dissolution did not occur in the 12Y1.

Differences in the microstructures of 12Y1 and 12YWT were reflected in the differences in tensile (Fig. 2) and creep-rupture (Fig. 6) strengths, with the 12YWT having much higher tensile and creep-rupture strengths than 12Y1. The yield stress of the 12YWT was also significantly higher than that of the commercial MA956 and PM 2000, and it was comparable to that of MA957 (Fig. 4).

The difference in creep-rupture properties of the commercial steels and 12YWT did not follow from the relative strengths observed in the tensile tests. In particular, although 12YWT had the highest yield stress and ultimate tensile strength of the experimental steels and all the commercial steels but MA957 (Fig. 4), creep-rupture properties based on the LMP comparison indicated that in the limit of low stresses (long rupture times) and/or high test temperatures, the commercial steels and the 12YWT are expected to approach a common strength level (Fig. 10).

The MA956 had yield stress and ultimate tensile strength values from room temperature to 800 °C that were much less than those for 12YWT. Although at the higher LMPs, the MA956 had lower creep-rupture strength than 12YWT, for long-time tests and/or high-temperature creep tests, the values for MA956 approached those for 12YWT. Part of the difference in tensile properties could be reflected in the difference in grain size and the amount of recrystallized structure. Although no grain-size measurements were attempted because of the high anisotropy and because some of the steels were not completely recrystallized, it was obvious that the grain size of the MA956 was the largest of any of the steels, and this steel appeared to be completely recrystallized (Fig. 11(a)). A completely recrystallized structure will have a lower dislocation density, and thus, a lower strength. Likewise, in accordance with the Hall–Petch relationship, the larger grain size of the MA956 will contribute to a lower yield stress.

Similarly, the yield stress and ultimate tensile strength of PM 2000 were less than for 12YWT – probably due to the presence of more unrecrystallized material in the 12YWT – but the long-time, low-stress creep-rupture properties determined at ORNL on PM 2000 0.08- and 0.13-mm sheet specimens were as good as those for the 12YWT (Fig. 8). Note that the tensile properties in Fig. 4 for PM 2000 are from vendor data on bar product, and the ORNL creep tests were on sheet at 850–1000 °C. Vendor data for ultimate tensile strength (no yield stress data were given) for 1–8-mm sheet showed the sheet to be weaker than the bar [15]. A similar strength difference was present in the vendor creep-rupture data for bar and sheet (Fig. 9). These latter high-LMP data, determined at higher temperatures (900–1150 °C) than the ORNL data for the MA957 (800–925 °C) and the two experimental steels (600–900 °C), show the same trend with increasing LMP as that of the MA956 (determined at 800–1200 °C). The vendor creep-rupture data for MA956 and PM 2000 at high LMP appear to have similar slopes and therefore define a band. The difference between the PM 2000 bar and sheet could be an effect of the amount of recrystallized material and/or a grain-size effect.

Finally, the MA957 and 12YWT had equivalent yield stresses and ultimate tensile strengths. The explanation for this must be found in the microstructure comparison, which will be discussed below. Comparison of the LMP for these two steels indicated that for the completed creep tests for MA957, there was an advantage for 12YWT (Fig. 7). However, these were relatively high-stress, low-temperature (low LMP) tests, and just as for the other commercial products, at high LMP the values for MA957 approached those for MA956, which appear to converge with those for 12YWT.

These results indicate that, with the exception of 12Y1, the creep-rupture properties of the other four steels approach a similar strength level with decreasing creep-rupture stress and/or increasing test temperature

(high LMP). As stated above, the excellent creep strength of the 12YWT relative to 12Y1 was caused by the fine distribution of particles (atom clusters) and unrecrystallized material in the 12YWT [6–9]. Recent atom-probe studies on the MA957 indicated the presence of 2-nm-diameter particles similar to those in 12YWT [17]. Just as in 12YWT, the particles were rich in Ti, Y, and O. These results indicate that the same dissolution of the Y_2O_3 that occurred during mechanical alloying in 12YWT [9,17] also occurred during mechanical alloying of MA957. Since the creep properties of these steels depend on the distribution of oxide particles, the convergence of rupture properties at long times would be expected, given the similarity of the microstructures.

Given the convergence of creep-rupture properties of MA956, MA957, PM 2000, and 12YWT at long rupture time and/or high temperatures (Fig. 10), one explanation is that the MA956 and PM 2000 also contain the high density of small particles found in MA957 and 12YWT. As stated above, the dissolution of Y_2O_3 in 12YWT and not in 12Y1 was attributed to the presence of titanium in the 12YWT and not in 12Y1. The MA957, which also had the atom clusters, contained titanium, as do MA956 and PM 2000 (Table 1), thus enhancing the possibility that fine atom clusters form in these latter two steels.

Generally, relative creep strengths are comparable to relative strengths observed in a tensile test. Therefore, at first glance, it appears there may be a problem with the explanation that the similarity of creep-rupture behavior of the 12YWT and the commercial steels is caused by similar nano-sized particles. Although there was an approach of the tensile properties at high temperatures for all the steels, there was a relatively large difference in tensile properties at lower test temperatures (Fig. 4).

From optical microscopy, TEM, and atom-probe observations on the 12Y1 and 12YWT, it appeared that the major microstructural differences in the two was the absence of small nano-sized clusters in 12Y1 [6,8,9] and a larger amount of unrecrystallized material in 12YWT. These observations were used above to explain why 12Y1 has inferior tensile and creep-rupture properties compared to 12YWT. The observation of nano-sized clusters in the MA957 [17] and some unrecrystallized material also explains the similarity in tensile and creep properties of this steel and 12YWT. All indications are that the MA 956 examined here is completely recrystallized, although this was not necessarily the MA 956 for which the literature data are plotted in the figures. Therefore, even if all the commercial steels contain the nano-sized clusters postulated above and tensile and creep properties are determined by these particles, then all the commercial steels might be expected to have similar tensile properties over the entire test temperature range, which was not the case.

As discussed above, the yield stress and ultimate tensile strength for all the steels converged at the highest test temperatures, although the 12Y1 had the lowest values at the highest temperatures (Fig. 4). Convergence for this steel appeared to be at a much higher temperature than for the other steels. If it is assumed that 12YWT, MA956, MA957, and PM 2000 all contained a similar fine distribution of nano-size particles, and since the approach of properties occurs for long-time, high-temperature creep-rupture tests, it probably means that the fine particles determine the creep-rupture properties under these conditions. This follows because dislocation recovery and/or recrystallization can occur during the test at increasing rates with increasing temperature. Note that the vendor tests on MA 956 [12] and PM 2000 [15] were at temperatures up to 1200 °C, considerably higher than for the ORNL tests on 12YWT [7], MA 957 [10], and PM 2000 [11]. This means the unrecrystallized material has a large effect on the low-temperature tensile properties, but it has a decreasing effect on the properties as the test temperature is increased. It also means that the hardening by the small atom clusters does not play a major role in the tensile properties at the lower temperatures.

This explanation can account for the approach of the yield stress and ultimate tensile strength of all the steels in elevated-temperature tests. It also explains why the 12Y1 has inferior tensile and creep properties compared to the other steels. Namely, the 12Y1 contains fewer particles and they are larger than those in the other steels. Furthermore, the band of data in the stress-LMP curves observed for the highest LMPs for the MA956 and the PM 2000 bar and sheet (Fig. 10), may then be explained by differences in grain size. Detailed SEM, TEM, and quantitative optical microscopy studies are required to determine if these hypotheses can be correlated with the mechanical properties observations.

The above discussion assumed creep occurred by a dislocation mechanism where creep rate is determined by the climb and glide of dislocations through the distribution of oxide particles (power-law creep). For this mechanism, the steady-state creep rate is given by

$$\dot{\varepsilon} = k\sigma^n,$$

where $\dot{\varepsilon}$ is the creep rate, σ is the stress, and k and n are constants. For dislocation climb and glide mechanisms, the stress exponent n has values of 3 or higher. Values of 10 and higher are found for some dispersion-strengthened materials. However, as the stress is lowered and/or the temperature is increased, the creep mechanism eventually changes to grain-boundary sliding, diffusion creep, and/or Harper–Dorn creep, and the value of n is reduced to 1–2. Under what test conditions this change occurs depends on the material. A detailed creep testing program is required to determine the stress–temperature regimes for the different mechanisms, which can be rep-

resented on deformation-mechanism maps [25,26]. No such map is available for ODS steels.

The convergence of the Larson–Miller parameters of the different ODS steels at high Larson–Miller parameters (high temperature and long rupture time) as stress decreases might indicate a change to a creep mechanism with less dependence on the oxide-particle distribution. Again, the band of creep-rupture properties at high LMP values could signify an effect of grain size. More creep testing is required to verify if there was a change in the creep mechanism with increasing LMP.

5. Summary and conclusions

Tensile and creep-rupture data for two experimental and three commercial ODS steels were compared. Experimental steels are: 12Y1 (nominally Fe–12Cr–0.25Y_2O_3) and 12YWT (Fe–12Cr–3W–0.4Ti–0.25Y_2O_3); commercial steels are: MA956 (Fe–20Cr–4.5Al–0.33Ti–0.5Y_2O_3), MA957 (Fe–14Cr–0.3Mo–1Ti–0.25Y_2O_3), and PM 2000 (Fe–19Cr–5.5Al–0.5Ti–0.5Y_2O_3).

A significant variation in the yield stress and ultimate tensile strength of the different steels occurred for tests at room temperature to 800 °C. The 12YWT was much stronger than the 12Y1. Of the commercial steels, MA957 was the strongest with properties similar to those of 12YWT. The MA956 was the weakest of the commercial steels; it was also weaker than 12Y1 below 650 °C. The PM 2000 had a strength between that of MA956 and MA957; up to ≈550 °C, the strength of PM 2000 was comparable to that of 12Y1, but at higher temperatures, PM 2000 was substantially stronger. Strength properties of all steels appeared to merge for extrapolations above ≈900 °C.

Creep-rupture properties were compared using a Larson–Miller parameter with a constant of 25. Properties of the PM 2000 sheet tested at ORNL were similar to the 12YWT over all the test temperatures common to the two steels. Although the 12YWT had better creep-rupture properties than MA956 and MA957 for high stresses and low Larson–Miller values, at high Larson–Miller parameters (high-temperature, long rupture life) there appeared to be a convergence of properties. Larson–Miller parameters for 12YWT, PM 2000, MA956, and MA957 were greater than those for 12Y1 at all stresses.

The reason for the similar tensile and creep behavior of MA957 and 12YWT was concluded to be the distribution of nano-sized particles rich in Y, Ti, and O observed by TEM and atom probe studies on the two steels. In contrast, such studies found much larger Y_2O_3 particles in the weaker 12Y1, explaining why this steel had inferior tensile and creep properties. Although it was postulated that the excellent long-term, high-temperature creep properties of MA956 and PM 2000 was also due to the presence of a fine distribution of nano-size particles, more work is required to verify this.

Acknowledgments

We wish to thank the following people who helped in the completion of the experimental work: J.R. Mayotte carried out the optical metallography and B.L. Sparks conducted the creep tests. Drs S.J. Zinkle, R.O. Stoller, and M.A. Sokolov reviewed the manuscript and provided helpful comments.

This research was performed as part of the International Nuclear Energy Initiative (I-NERI) program for the Office of Nuclear Energy, Science and Technology, US Department of Energy in collaboration with the French Commisariat a l'Energie Atomique (CEA) and sponsored in part by the Office of Fusion Energy Sciences, US Department of Energy, under contract DE-AC05-00OR22725 with UT-Battelle, LLC.

References

[1] S. Ukai, T. Nishida, H. Okada, T. Okuda, M. Fujiwara, K. Asabe, J. Nucl. Sci. Technol. 34 (1997) 256.
[2] S. Ukai, T. Yoshitake, S. Mizuta, Y. Matsudaira, S. Hagi, T. Kobayashi, J. Nucl. Sci. Technol. 36 (1999) 710.
[3] A. Alamo, J. Decours, M. Pigoury, C. Foucher, Structural Applications of Mechanical Alloying, ASM International, Materials Park, OH, 1990.
[4] A. Alamo, H. Regle, G. Pons, L.L. Bechade, Mater. Sci. Forum 88–90 (1992) 183.
[5] D.K. Mukhopadhyay, F.H. Froes, D.S. Gelles, J. Nucl. Mater. 258–263 (1998) 1209.
[6] M.K. Miller, E.A. Kenik, K.F. Russell, L. Heatherly, D.T. Hoelzer, P.J. Maziasz, Mater. Sci. Eng. A 353 (2003) 140.
[7] R.L. Klueh, P.J. Maziasz, I.S. Kim, L. Heatherly, D.T. Hoelzer, N. Hashimoto, E.A. Kenik, K. Miyahara, J. Nucl. Mater. 307–311 (2002) 773.
[8] I.-S. Kim, J.D. Hunn, N. Hashimoto, D.L. Larson, P.J. Maziasz, K. Miyahara, E.H. Lee, J. Nucl. Mater. 280 (2000) 264.
[9] D.J. Larson, P.J. Maziasz, I.-S. Kim, K. Miyahara, Scr. Met. 44 (2001) 359.
[10] R.L. Klueh, J.P. Shingledecker, unpublished research, 2003.
[11] B.A. Pint, R.W. Swindeman, K.L. More, P.F. Tortorelli, in: Proceedings of International Gas Turbine & Aeroengine Congress & Exhibition, New Orleans, LA, 4–7 June 2001, American Society of Mechanical Engineers, New York, 2001.
[12] Engineering Data Sheet for Incoloy MA956, Special Metals Corp., SMC-008, October 2003.
[13] J.J. Fischer, US Patent 4,075,010,21, February 1978.
[14] M.L. Hamilton, D.S. Gelles, R.J. Lobsinger, G.D. Johnson, W.F. Brown, M.M. Paxton, R.J. Puigh, C.R.

Eiholzer, C. Martinez, M.A. Blotter, Fabrication Technological Development of the Oxide Dispersion Strengthened Alloy MA957 for Fast Reactor Applications, Pacific Northwest National Laboratory, PNNL-13168, February 2000.
[15] Material Data Sheet ODS-Superalloy PM 2000, Metallwerk Plansee GmbH, February 1993.
[16] R.L. Klueh, Metall. Trans. 20A (1989) 463.
[17] M.K. Miller, D.T. Hoelzer, E.A. Kenik, K.F. Russell, J. Nucl. Mater. 329–333 (Part 1) (2004) 338.
[18] J.-J. Huet, H. Massaux, L. DeWilde, J. Noels, Rev. Métall. 65 (1968) 12.
[19] M.L. Hamilton, D.S. Gelles, R.J. Lobsinger, G.D. Johnson, W.F. Brown, M.M. Paxton, R.J. Puigh, C.R. Eiholzer, C. Marinez, M.A. Blotter, Oxide Dispersion Strengthened Alloy MA957 for Fast Reactor Applications, Pacific Northwest National Laboratory, PNNL-13168, February 2000.
[20] S. Ukai, S. Mizuta, M. Fujiwara, T. Okuda, T. Kobayashi, J. Nucl. Sci. Tech. Mater. 39 (2002) 778.
[21] S. Ukai, T. Okuda, M. Fujiwara, T. Kobayashi, S. Mizuta, H. Nakashima, J. Nucl. Sci. Tech. Mater. 39 (2002) 872.
[22] M.J. Alinger, G.R. Odette, G.E. Lucas, J. Nucl. Mater. 307–311 (2002) 484.
[23] S. Ukai, M. Fujiwara, J. Nucl. Mater. 307–311 (2002) 749.
[24] T. Okuda, M. Fugiwara, J. Mater. Sci. Lett. 14 (1995) 1600.
[25] M.F. Ashby, C. Gandhi, D.M.R. Taplin, Acta Metall. 27 (1979) 669.
[26] H.J. Frost, M.F. Ashby, Deformation – Mechanism Maps, Pergamon Press, Oxford, England, 1982.